A Coupled Car-Parrinello Molecular Dynamics and EXAFS Data Analysis Investigation of Aqueous Co²⁺

Riccardo Spezia,[†] **Magali Duvail,**[†] **Pierre Vitorge,**[†,‡] **Thierry Cartailler,**[†] **Jeanine Tortajada,**[†] **Giovanni Chillemi,**[§] **Paola D'Angelo,**[*,#] **and Marie-Pierre Gaigeot**[*,†,^]

Laboratoire Analyse et Modélisation pour la Biologie et l'Environnement, UMR-CNRS 8587, Université d'Evry Val d'Essonne, Boulevard F. Mitterrand, 91025 Evry Cedex, France, CEA Saclay, DEN, DPC, SECR, LSRM, 91991 Gif Sur Yvette, France, CASPUR, Inter-University Consortium for Supercomputing in Research, via dei Tizii 6b, 00185 Roma, Italy, Dipartimento di Chimica, Università di Roma "La Sapienza", P.le Aldo Moro 5, 00185 Roma, Italy, and LPTMC, Université Pierre et Marie Curie-Paris 6, UMR-CNRS 7600, 4 Place Jussieu, Case courrier 121, 75052 Paris, France

Received: July 24, 2006

We have studied the microscopic solvation structure of Co²⁺ in liquid water by means of density functional theory (DFT)-based Car−Parrinello molecular dynamics (CPMD) simulations and extended X-ray absorption fine structure (EXAFS) data analysis. The effect of the number of explicit water molecules in the simulation box on the first and second hydration shell structures has been considered. Classical molecular dynamics simulations, using an effective two-body potential for Co²⁺−water interactions, were also performed to show box size effects in a larger range. We have found that the number of explicit solvent molecules has a marginal role on the first solvation shell structural parameters, whereas larger boxes may be necessary to provide a better description of the second solvation shell. Car−Parrinello simulations were determined to provide a reliable description of structural and dynamical properties of Co²⁺ in liquid water. In particular, they seem to describe both the first and second hydration shells correctly. The EXAFS signal was reconstructed from Car−Parrinello simulations. Good agreement between the theoretical and experimental signals was observed, thus strengthening the microscopic picture of the Co²⁺ solvation properties obtained using first-principle simulations.

1. Introduction

Knowledge of the hydration structure of transition-metal ions in aqueous solution is of fundamental importance to understand their solvation properties and chemical reactivities. A large number of studies have been performed on this topic, both experimentally[1−3] and theoretically.[4,5] From the theoretical point of view, molecular dynamics (MD) and Monte Carlo simulations are the preferential modeling techniques to provide a microscopic picture of ionic solutions. Because of their relatively low computational cost, classical MD simulations have been used intensively in the past years.[6−12] Recently, effective ion−water two-body classical potentials have been developed, starting from quantum mechanical ab initio calculations in which the many-body ion−water terms are accounted for by the polarizable continuum model.[13−15] However, all the classical MD methods suffer the limitation of transferability, because a given potential cannot be used to describe different metal−solvent interactions or weakly binding interactions of the metal with other ligand molecules that can be present in solution. In fact, a major interest in modeling transition metals in solution is aimed at the

understanding of interactions, not only with the solvent but also with other coordinating molecules.

Classical potential limitations can be circumvented by performing electronic structure calculations. Among these methods, Car−Parrinello molecular dynamics (CPMD) simulations—based on density functional theory (DFT)—provide such a theoretical framework; this methodology has become very popular in the past 10 years. These simulations can be applied in gas,[16−18] liquid,[19−21] and solid[22,23] phases.

CPMD simulations have been reported in the literature for several metal ions in aqueous solution, namely Li⁺,[24] Be²⁺,[25] Na⁺,[26−28] Mg²⁺,[29] Al³⁺,[30] K⁺,[31] Ca²⁺,[32] Fe²⁺,[33,34] Cu²⁺,[35] Ag⁺,[27] Fe³⁺,[36] Cr³⁺,[37] and Co³⁺,[38] with varying degrees of success. CPMD simulations of anions and neutral metal atoms in solution have also been published, such as, for example, the study of bromide ion solvation reported by Raugei and Klein[39] and the neutral silver dipolar atom in water reported by Spezia et al.[40]

X-ray absorption spectroscopy (XAS) is a very powerful technique to shed light onto the hydration structure of metal cations,[41] and, in particular, to investigate the short-range environment around selected atomic species in condensed matter. Because of the broad correlation function toward the large distances and to the finite mean-free path of the photo-electron, the sensitivity of extended X-ray absorption fine structure (EXAFS) is limited to the neighborhood (∼4−5 Å) of the photoabsorber atom. Although the experimental characterization of disordered systems over the full range of distances is hampered by the short-range sensitivity, EXAFS has been

---

* Authors to whom correspondence should be addressed. E-mail addresses: p.dangelo@caspur.it, gaigeot@ccr.jussieu.fr.
† Laboratoire Analyse et Modélisation pour la Biologie et l'Environnement, UMR−CNRS 8587, Université d'Evry Val d'Essonne.
‡ CEA Saclay, DEN, DPC, SECR, LSRM.
§ CASPUR, Inter-University Consortium for Supercomputing in Research.
# Dipartimento di Chimica, Università di Roma "La Sapienza".
^ LPTMC, Université Pierre et Marie Curie-Paris 6, UMR−CNRS 7600.

proven to provide structural information on the first hydration shell of ionic solutions, which is not possible with other experimental techniques.[6,42−44] The XAS chemical selectivity is of particular interest, because it allows one to examine complex systems (those containing a large number of atoms) and diluted samples. For such systems, it appears that, very often, XAS is the only structural tool that can be profitably used. Moreover, whereas pair distribution functions can also be obtained by diffraction techniques, EXAFS spectroscopy offers a unique opportunity to determine higher-order correlation functions that describe the ion−solvent associations that exist in solution.[42,43,45] Recent investigations conducted on aqueous solutions of 3d metal ions have shown that the EXAFS technique can be used to assess the reliability of structural results obtained from computer simulations.[46] The combination of MD simulations and EXAFS spectroscopy is a well-known performing "tandem" technique to unravel the structure of ionic solutions, especially for metal cations in a disordered environment.[6,7,46,47] Reconstruction of the EXAFS signal using computer simulations is generally performed from classical MD data.[41] To the best of our knowledge, only one Born−Oppenheimer ab initio MD study of liquid $In_{100−x}Se_x$ alloys has been reported in the literature[48] to reconstruct the EXAFS signal using the multiple-scattering (MS) theory.

In the present work, we report a direct comparison between Car−Parrinello molecular dynamics (CPMD) simulations and EXAFS, based on the reconstruction of the experimental signal using MS theory. To the best of our knowledge, this is the first time that such a comparison is made to understand the hydration structure of ions in solution. The EXAFS theoretical signal was calculated using the two-body and three-body distribution functions obtained from CPMD simulations, and it was compared to the experimental data without any fitting procedure. This CPMD−EXAFS combined approach has been applied to the study of the Co^{2+} hydration structure to assess the reliability of our computational scheme. Understanding cobalt behavior in aqueous solution is an important theoretical question that is related to its toxicological activity. This metal, which is needed at trace level in organisms for the bio-synthesis of vitamin B12, is a typical polluting agent issued from several industrial processes. It is also an important radioactive contaminating species, especially the ^{60}Co isotope. Thus, we have begun combined theoretical and experimental studies of cobalt properties in biologically and environmentally relevant systems.[17,49] As a result of our previous theoretical efforts, we have demonstrated the validity of Co^{2+} pseudo-potential and Car−Parrinello setup in describing Co−cysteine, Co−gluthation and Co−water interactions in the gas phase.[17] In regard to the Co^{2+} hydration structure, here, we report a study aimed at assessing the reliability of CPMD simulations in reproducing EXAFS data for Co^{2+} in liquid water. Recent experimental EXAFS studies were performed by some of us.[46] An effective two-body classical Co^{2+}−water potential was developed[13] to study Co^{2+} solvation. Moreover, a quantum mechanics/molecular mechanics (QM/MM) MD study of aqueous Co^{2+} was recently presented by Rode's group, which provided another independent benchmark for our study.[50]

The outline of the reminder of the text is as follows. In sections 2.1 and 2.2, we describe the Car−Parrinello and classical MD setups, respectively, whereas in section 2.3, we present the EXAFS measurements and data analysis details. Results are presented in section 3, divided into solvation structure description (section 3.1), and reconstruction of the EXAFS signal from MD data compared with experiments

(section 3.2). The behavior of first and second hydration shells is discussed in section 4.1 and 4.2, respectively. Finally, in section 5, we summarize our work and draw some conclusions.

2. Methods

2.1. Car−Parrinello Molecular Dynamics (CPMD). We performed CPMD simulations[51,52] of the Co^{2+} ion immersed in liquid water. Two cubic boxes of different dimensions were considered, consisting of 32 (cubic edge of 9.87 Å) and 64 (cubic edge of 12.42 Å) water molecules, respectively. The box dimension is chosen to reproduce the water density at 300 K. Periodic boundary conditions were applied. The electronic structure of the valence electrons was described by DFT using the BLYP functional[53,54] within the local spin density (LSD) representation. The Co^{2+} ion was considered in a quartet state, corresponding to the experimental spin state,[55] and to previous calculations within the framework of a continuum description of the solvent.[13] The valence electron wave function was expanded in plane waves with an energy cutoff of 90 Ry. This relatively high value is needed to ensure energy convergence, as we have recently reported.[17] Note that this requirement makes our CPMD calculations more computationally expensive, in comparison to other simulations of metal cations in bulk water, where the plane wave cutoff used was slightly lower (in the range of 60−80 Ry).[36,38]

Medium soft norm-conserving pseudopotentials of the Trouillier−Martins type[56] were used. Standard Trouillier−Martins pseudopotentials of O and H atoms were used, as in several Car−Parrinello studies. The electronic structure of Co^{2+} is $[Ar]3d^74s^0$. Thus, as reported by Rovira et al.[57] and by some of us,[17] the adopted cobalt pseudopotential retains only the $3d^7$ and $4s^0$ electronic levels as valence states. Other details on the Co^{2+} pseudopotential parameters and their validation have been reported elsewhere.[17] Energy expectations were calculated in reciprocal space using the Kleinman−Bylander transformation.[58] We also applied nonlinear core correction[59] (with a core-charge radius of 1.2 au) which partially accounts for the nonlinearity in the exchange-correlation potential. This is especially recommended for transition metals.

All Car−Parrinello simulations were conducted with the program package CPMD[60] in the NVE ensemble. Initial configurations were obtained from 2 ps equilibrated CLMD of the solute−solvent system (see next subsection for details). The system was subsequently equilibrated via 1 ps CPMD with initial velocities obtained from a Maxwell distribution centered on 300 K. Car−Parrinello data were then collected over 5 ps of simulation runs, without control of the temperature. The average temperature was 293 ± 10 K. We used a relatively small fictitious electron mass of 400 au to improve the bulk water description, as recently suggested by Galli et al.[61] in their studies of pure liquid water. Moreover, as previously done by some of us,[17] we used a time step of 4 au (0.097 fs), which is smaller, with respect to other CPMD simulations of metal cations in liquid water.

The two sets of CPMD simulations, using 32 and 64 water molecules in the simulation box (with periodic boundary conditions), will be referenced hereafter as CPMD-32 and CPMD-64, respectively. We also will be using our gas-phase dynamical structure of a $[Co(H_2O)_6]^{2+}$ cluster from our previous Car−Parrinello simulation data of ref 17. It will be referenced hereafter as CPMD-6.

2.2. Classical Molecular Dynamics (CLMD). CLMD of Co^{2+} in aqueous solution were performed using boxes with an increasing number of water molecules. We used 32, 64, 216,

and 1000 water molecules in the NVE ensemble, applying periodic boundary conditions to simulate bulk systems. Long-range interactions were treated using the Ewald summation method.[62] The system was equilibrated at 300 K for 2 ps. Production runs were subsequently collected for 1 ns. Newton's equations of motion were solved numerically with the velocity Verlet algorithm, using a time step of 1 fs. Dynamics were performed with our own developed code.[63] The SPC/E water model was used,[64] and Co^{2+}−water interaction energies were evaluated using the effective two-body potential recently proposed by Chillemi et al.:[13]

$$V = \sum_I \left(\frac{q_{Co}q_I}{r_{CoI}} + \frac{A_I}{r_{CoI}{}^4} + \frac{B_I}{r_{CoI}{}^6} + \frac{C_I}{r_{CoI}{}^8} + \frac{D_I}{r_{CoI}{}^{12}} \right) + E_O e^{-F_0 r_{CoO}}$$

(1)

where *I* runs over O and H atoms, whereas the exponential contribution is added only for oxygen. Parameters were fitted to the Co^{2+}−water ab initio potential energy surface, where the many-body ion−water terms were taken into account by means of the conductor-like polarizable potential method,[65] as presented in ref 13.

In the following discussion, we will refer to the 32-, 64, 216-, and 1000-molecule classical simulations as CLMD-32, CLMD-64, CLMD-216, and CLMD-1000, respectively. We recall that Chillemi et al.[13] have performed CLMD simulations of Co^{2+} in a box of 819 water molecules, using the same force field, in the NVT ensemble, using a cutoff for treating long-range interactions. In the following discussion, we will refer to this simulation as CLMD-819.

2.3. Extended X-ray Absorption Fine Structure (EXAFS) Measurements and Data Analysis. *2.3.1. EXAFS Measurements.* A 0.2 M Co^{2+} aqueous solution was obtained by dissolving the appropriate amount of Co(NO$_3$)$_2$ in freshly distilled water that was acidified to pH ∼2.5 by adding HNO$_3$. The EXAFS spectrum at the Co K-edge was recorded in transmission mode, using the EMBL spectrometer at DESY.[66] Measurements were performed at room temperature with a Si(220) double-crystal monochromator and 50 % harmonic rejection achieved by slightly detuning the two crystals from parallel alignment.[67] Three spectra were recorded and averaged after performing an absolute energy calibration.[68] The DORIS III storage ring was running at an energy of 4.4 GeV with positron currents between 70 mA and 40 mA. The solution was kept in a cell with Kapton film windows and a Teflon spacer of 1 mm.

2.3.2. Data Analysis. The relation between the EXAFS $\chi(k)$ signal and the local structure, defined through the *n*-body distribution functions, contains the integrals of the two-atom ($\gamma^{(2)}$), three-atom ($\gamma^{(3)}$), and *n*-atom ($\gamma^{(n)}$) signals, which can be calculated using the multiple-scattering (MS) theory.[69] In "conventional" EXAFS data analysis of disordered systems, only two-body distributions are considered, and the $\chi(k)$ signal is represented by the equation

$$\chi(k) = \int_0^\infty 4\pi\rho r^2 g(r)A(k,r)\sin[2kr + \phi(k,r)]\,dr \quad (2)$$

where $A(k,r)$ and $\phi(k,r)$ are the amplitude and phase functions, respectively, and ρ is the density of the scattering atoms. Recent investigations have shown that MS effects within the first hydration shell must be accounted for to perform an accurate analysis of the EXAFS spectra of transition-metal ions in aqueous solution.[42,46] MS contributions are detectable for Co^{2+}, because 3d transition-metal ions form very stable octahedral

complexes, at variance with alkaline and alkaline-earth ions, which have highly diffuse and poorly defined hydration spheres. $\chi(k)$ theoretical signals can be calculated by introducing into eq 2 the model radial distribution functions (RDFs) obtained from CLMD or CPMD simulations. Both the Co−O and Co−H $g(r)$ distributions obtained from the simulations have been used to calculate the single scattering first shell $\chi(k)$ theoretical signal, because the ion−hydrogen interactions have been determined to provide a detectable contribution to the EXAFS spectra of transition-metal ions in aqueous solutions.[46] Moreover, we have included the three-body contributions within the first hydration shell. The strongest MS signals are generated by the three linear O−Co−O scattering paths in the octahedral hydration complex. Therefore, we have also considered the contributions associated with the $g(r_1,r_2,\theta)$ distributions obtained from CPMD simulations. The orientation of water molecules in the first coordination shells has been obtained from the analysis of the O−Co−O triangular configurations that show well-defined peaks at $\theta \simeq 90°$ and $\theta \simeq 180°$, in agreement with the expected octahedral coordination of this ion. Comparison of the theoretical and experimental total $\chi(k)$ signals allows the reliability of the $g(r)$ distributions and, consequently, that of the theoretical scheme used in the simulations, to be checked.

The EXAFS theoretical signals associated with all the two- and three-body distributions have been calculated by means of the GNXAS program, and a thorough description of the theoretical framework for the multiple scattering analysis can be found in ref 69. Phase shifts, $A(k,r)$, and $\phi(k,r)$, have been calculated starting from one of the CLMD-819 configurations as previously reported,[46] using muffin-tin potentials and advanced models for the exchange-correlation self-energy (Hedin−Lundqvist).[70] The values of the muffin-tin radii are 0.2, 0.9, and 1.2 Å for hydrogen, oxygen, and cobalt, respectively. Inelastic losses of the photoelectron in the final state have been intrinsically accounted for by complex potential. The imaginary part also includes a constant factor accounting for the core-hole width (1.33 eV).[71]

It is well-known that the atomic background of several elements contains important contributions associated with the opening of multielectron excitation channels. Here, the background function used to extract the $\chi(k)$ experimental signals has been modeled by means of step-shaped functions accounting for the 1s 3p and 1s 3s double-electron resonances. The energy onsets and the intensities of these channels were taken from previous determinations.[46,72] The S_0^2 parameter, which accounts for an overall intensity rescaling, and E_0 which aligns the experimental and theoretical energy scales were taken from the analysis reported in ref 46.

3. Results

3.1. Solvation Structure. The Co^{2+} ion in aqueous solution is well-known to be coordinated by six water molecules,[55] and this hexa-coordinated structure is observed in all our simulations (both classical and DFT-based). A typical octahedral-like arrangement of water molecules in the Co^{2+} first hydration shell is shown in Figure 1.

Structural arrangements of water molecules around Co^{2+} are investigated by computing Co−O and Co−H RDFs, and the results are collected in Figure 2 for CPMD-32, CPMD-64, CLMD-32, CLMD-64, CLMD-216, and CLMD-1000. In the same figure, we show the Co−O and Co−H first shell RDFs obtained from the EXAFS analysis, with associated error bars.[46] Structural characterization of the first hydration shell is completed by O−Co−O angle distribution (see Figure 3). The
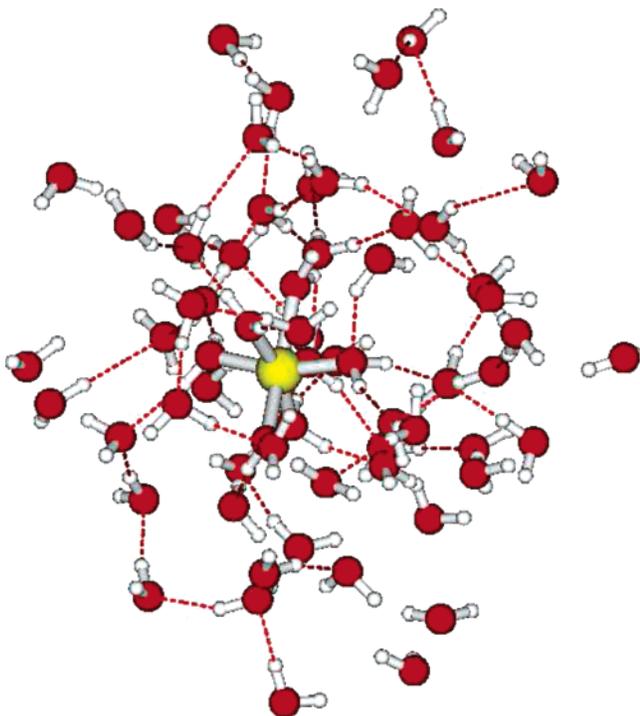
Figure 1. CPMD-64 snapshot showing a $[Co(H_2O)_6]^{2+}$ octahedral structure immersed in water.

second hydration shell is characterized through the Co−O second peak distances and the number of water molecules located on average in the second solvation shell. All these data are summarized in Table 1 together with previous theoretical results.[13,50]

The most evident feature in the Co−O $g(r)$ global behavior is that Car−Parrinello RDFs are less sharp than experimental functions, while their classical analogues are sharper (see Figure 2). This last feature was also found in previously reported CLMD.[13]

Differences between CPMD and the experimental data can be quantified by fitting the $g(r)$ first peaks with a typical gamma asymmetric distribution (see Appendix for details, and Table 2). Note that the R_m values reported in Table 2 are the average distances of the obtained distributions that are shifted toward larger values, with respect to the maximum of the $g(r)$ distributions of Table 1, which is due to the asymmetry of the distributions. CPMD simulations slightly overestimate the position of the first Co−O peak (2.15 Å in CPMD-32 and 2.14 Å in CPMD-64) in comparison to experiments (2.09 Å), even if a very small improvement in R_m is obtained by using a larger simulation box. Shorter distances and broader distributions are obtained from CPMD for Co−H distributions. Anyway, these differences, are always very small and of the same order of magnitude of what has been found from distribution peak analysis by other authors, using different simulation methods.[50]

In Figure 3, we show the distribution of O−Co−O angles, taking into account the first hydration shell water molecules, as obtained from Car−Parrinello simulations (CPMD-32 and CPMD-64). In both cases, we found two peaks (at ∼90° and ∼180°), corresponding to an octahedral structure (in particular, 89° and 170° for CPMD-32 and 90° and 175° for CPMD-64). Note that the 64-water-molecule simulation provides two peaks closer to the ideal values, probably because of the better description of outer hydration shells, which, consequently, provides a finest description of the first hydration shell structure.

Structural analysis is completed by examining the water molecules in the second hydration shell. In Figure 4, we show the number of water molecules in the second hydration shell (CN2), as obtained via CPMD and CLMD with increasing box sizes. The CPMD simulations with the small box (32 water molecules) clearly show that the second hydration shell is not sufficiently well-described with this small box and small number of water molecules, and that a larger box is necessary to obtain a better behaved distribution. In CLMD, we always obtain well-behaved (unimodal) and well-defined peaked distributions, probably because of the conjunction of the larger number of water molecules in the box and of the larger simulation time scales. We note that a more complete statistical sampling is useful to improve the second shell description, even with a small box size.

In CPMD-64 simulations, the most probable number of water molecules in the second hydration shell is 12, whereas in CLMD simulations, this probability function is centered at 11 water molecules; with large values of the probability also for CN2 = 12, but always smaller than for CN2 = 11, as shown in the same figure (Figure 4). The mean coordination numbers, which are shown in Table 1, are, thus, on average, 12.5 for CPMD-64 and ∼11 for all CLMD.

3.2. EXAFS Signal from Car−Parrinello Dynamics. As shown in the previous section, the CPMD-32 and CPMD-64 simulations present only slight differences in the shape and position of the Co−water first shell RDFs. In both cases, the Co−O first peak distances are slightly longer, in comparison to the EXAFS experimental determination. Moreover, the mean-square variation factors (σ^2) and the asymmetry of the first shell peak obtained from the CPMD simulations are slightly too large. It is well-known that EXAFS investigations on ionic solutions can provide not only reliable short-range structural properties but also information on the ligand exchange process in the first hydration shell. Sham was the first to note that the ligand-exchange rate constant in a water solution of 3d metal ions is closely related to the EXAFS Debye−Waller factor.[73] More recently, Miyanaga et al.[74] showed that the σ^2 values do not reflect the real ligand exchange but rather the strength and stiffness of the ion-oxygen first shell bond. Therefore, the first conclusion that can be drawn is that the CPMD simulations does not reproduce the kinetic stability of the $[Co(H_2O)_6]^{2+}$ complex very accurately. This can be due to both the short simulation time and the theoretical model used (in particular, the functional or the atomic pseudopotential).

These discrepancies notwithstanding, direct comparison of the CPMD results with the EXAFS experimental data allows a better understanding of the accuracy of the simulations. $\chi(k)$ theoretical signals have been calculated using eq 2, starting from the CPMD-32 and CPMD-64 Co−O and Co−H $g(r)$ distributions. The linear and rectangular O−Co−O three-body contributions have been calculated using the angle values obtained from the analysis of the CPMD angular distribution. The average angle values and angle variances (σ_θ^2) were determined to be 170° and 12°, and 175° and 12° for the CPMD-32 and CPMD-64 simulations, respectively. The structural parameters derived from the CPMD simulations were kept fixed during the EXAFS analysis. In this way, the first hydration shell structure obtained from the simulations can be directly compared with experimental data and the validity of the theoretical framework used in the simulations can be assessed. In the upper panels of Figure 5, the comparison between the EXAFS experimental signal and the theoretical curves calculated using the CPMD-32 and CPMD-64 $g(r)$ distributions (the left and right
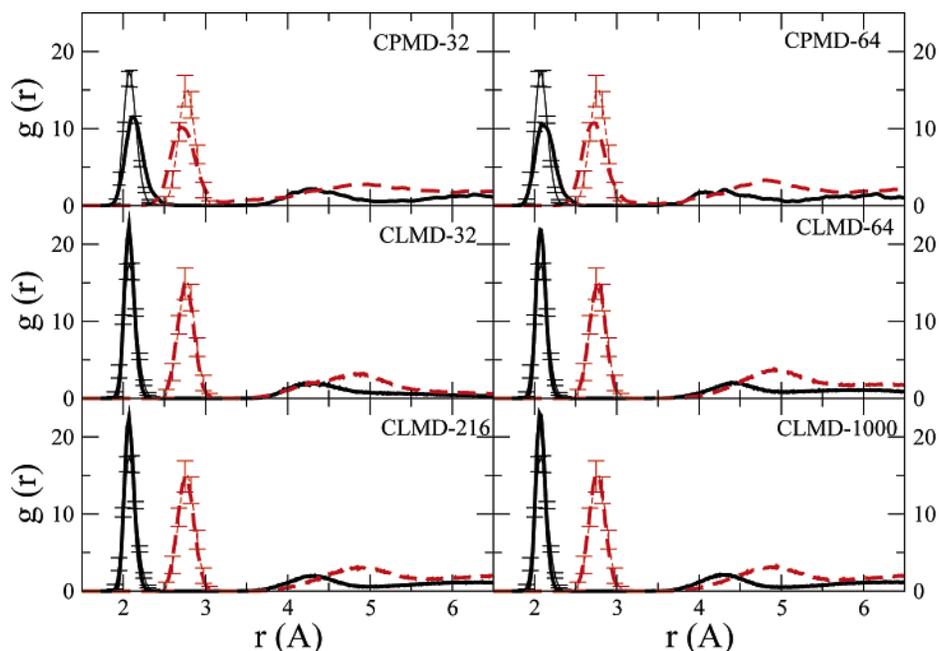
Figure 2. Co-O (thick lines) and Co−H (dashed lines) radial distribution functions (RDFs) obtained from different MD simulations: CPMD-32, CPMD-64, CLMD-32, CLMD-64, CLMD-216, and CLMD-1000. (See text for explanation of the abbreviations.) Experimental $g(r)$ distribution evaluated for the first shell from EXAFS measurements[46] are also reported, with associated errors, for comparison.
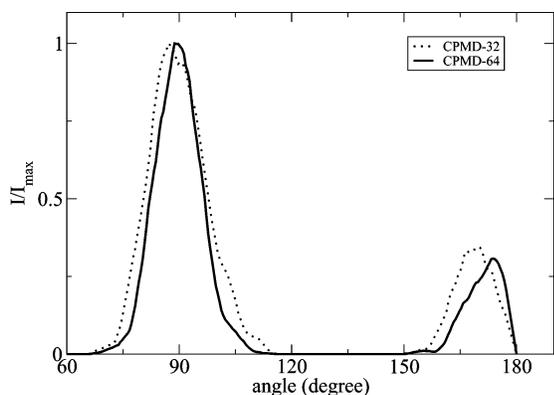

Figure 3. O−Co−O angle distributions obtained from CPMD-32 (dotted line) and CPMD-64 (solid line) simulations.

panels, respectively) is reported. The $\gamma^{(n)}$ signals are shown multiplied by k^2 for better visualization. The first four curves from the top of each panel are the Co−O and Co−H first shell $\gamma^{(2)}$ contributions, and the MS signals associated with the 3 linear and 12 orthogonal O−ion−O configurations. The reminder of the figures shows the total theoretical contributions, in comparison with the experimental spectra and the resulting residuals. As expected, the dominant contribution to the total EXAFS signal is given by the ion−O first shell signal and, as a consequence, the EXAFS structural information is particularly accurate only for the shape of the ion−O $g(r)$ distribution first peaks. The amplitude of both the Co−H two-body and MS contributions is below that of the residual curve. Overall, the calculated EXAFS spectra match the experimental data reasonably well in both cases, with R_i values of 0.721×10^{-6} and 0.707×10^{-6} for CPMD-32 and CPMD-64, respectively (see Appendix for the definition of this index of agreement). The agreement between the theoretical and experimental $\chi(k)$ signals shows that the structural and dynamical information derived from the CP simulations is basically correct and the size of the box does not affect the behavior of the first hydration shell. Note that the R_i value of the CPMD-64 simulation is only slightly smaller than that of the CPMD-32 simulation.

The Fourier transform (FT) moduli of the EXAFS $\chi(k)k^2$ theoretical, experimental, and residual signals are shown in the lower panels of Figure 5. The FTs have been calculated in the k-range of $2.1-13.5$ Å⁻¹ with no phase shift correction applied. The FT spectra show a prominent first shell peak, which is mainly due to the Co−O first shell distance. Nevertheless, the Co−H FT peaks are located at 2.4 Å, which creates a shoulder on the first peak. The very good agreement between the FTs of the theoretical and experimental signals again proves the reliability of the theoretical simulations.

4. Discussion

4.1. First Hydration Shell. We have shown that CPMD simulations provide a first shell Co²⁺ hydration structure that is in good agreement with EXAFS measurements, even if the theoretical $g(r)$ distributions are slightly wider and shifted toward longer distances. No box size effects were observed on the first hydration shell properties, because the CPMD-32 and CPMD-64 results are very similar—only angular distributions are slightly better using the larger box. Note that to obtain correct information on the first hydration shell qualitatively, the computationally less-expensive Car−Parrinello setup with 32 water molecules seems to be sufficient. Classical simulations, using an effective two-body metal-water potential, are able to provide better results, albeit preliminary accurate ab initio potential energy calculations are necessary. Nevertheless, CPMD simulations that have been performed using a BLYP DFT functional are able to reproduce these structural parameters quite well. Moreover, by recalculating the EXAFS signal from the CPMD $g(r)$ distributions, we obtain results that are very similar to the experimental results. Note that we did not perform any refinement of the theoretical $\chi(k)$ signal calculated from the CPMD data, because the background parameters have been taken from previous works.[46] The good agreement between the simulations and the experiments at this fine level of investigations makes the first-principle approach of CPMD simulations very intriguing, to understand the structure of soft matter around transition-metal cations. However, some differences were observed, indicating some

TABLE 1: Hydration Parameters for Co²⁺ in Aqueous Solution

	$r_{1Co-O}{}^a$ (Å)	$r_{1Co-H}{}^b$ (Å)	$r_{2Co-O}{}^a$ (Å)	CN-first^c	CN-second^c	$\theta_{O-Co-O}{}^d$ (°)
CPMD-6	2.14	2.82		6		87;173
CPMD-32	2.12	2.70	4.28	6	13.18 ± 0.95	89;170
CPMD-64	2.10	2.72	4.10	6	12.48 ± 1.29	90;175
CLMD-32	2.07	2.76	4.3	6	11.18 ± 1.54	90;174
CLMD-64	2.07	2.77	4.4	6	11.43 ± 1.43	90;173
CLMD-216	2.07	2.76	4.3	6	11.31 ± 1.28	90;175
CLMD-1000	2.07	2.76	4.3	6	11.48 ± 1.22	90;174
CLMD-819^e	2.08	2.78	4.29	6	12.7	90;174
CLMD-499^f	2.27	3.0	4.6	5.9	22.7	68;90;173
QM/MM^f	2.17	2.85	4.6	6	15.9	89;173

^{a} First (r_{1Co-O}) and second (r_{2Co-O}) peak maximum of Co−O $g(r)$ (in Å). ^{b} First peak maximum of Co−H $g(r)$ distribution (in Å). ^{c} Coordination number of the first (CN-first) and second (CN-second) hydration shell. ^{d} Peaks of the O−Co−O angular distribution function. ^{e} From ref 13. ^{f} From ref 50.

TABLE 2: Parameters of the First Peak $g(r)$ Fitted with a Gamma Distribution Function (See Appendix) Obtained from CPMD-32 and CPMD-64 Simulations and Compared with Previously Reported Classical Simulations (CLMD-819[13]) and Experimental Data[46]

parameter	Value			
	CPMD-32	CPMD-64	CLMD-819	EXAFS
	Co−O			
R_m (Å)	2.15	2.14	2.09	2.092(2)
σ^2 (Å²)	0.012	0.015	0.0038	0.0062(5)
β	0.4	0.4	0.3	0.3(1)
N	6.0	6.0	6.0	6.0(1)
	Co−H			
R_m (Å)	2.75	2.75	2.78	2.78(2)
σ^2 (Å²)	0.023	0.021	0.010	0.010(4)
β	0.3	0.4	0.0	0.05(9)
N	12.4	12.5	12.1	12.1(2)
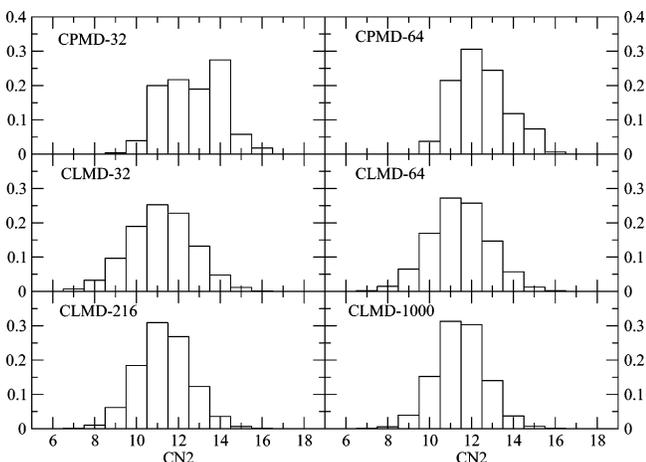
Figure 4. Histograms of water molecules in the second hydration shell of Co²⁺: (a) CPMD-32, (b) CPMD-64, (c) CLMD-32, (d) CLMD-64, (e) CLMD-216, and (f) CLMD-1000.

possible CPMD approach limitations, which may be overcome soon. The functional used, the pure BLYP, can be responsible for the longer Co−O distances and weaker bonds with corresponding broader distributions. Note that the calculated and experimental $\chi(k)k^2$ signals are almost identical up to 7 Å⁻¹, whereas the theoretical curve has a smaller amplitude in the higher range of k. This is reflected in a different amplitude of the FT of the $\chi(k)$ signal. These discrepancies are consistent with the broadening of the $g(r)$ distributions, as determined by the CPMD simulations previously outlined. However, differences between experimental and CPMD signals related to Co−O structure are very small and the position of the first peak in FT signal is not very affected. We should note that concentration and counterion effects can be also at the origin of these

differences. On the other hand, the shortening of the Co−H distances can be due both to the use of the BLYP functional and to an insufficient equilibration time. In fact, H atoms on the hexacoordinated water molecules should have a slow orientational relaxation time (more than tens of picoseconds[75]). Thus, our CPMD simulations do not sample these slow dynamics that are associated with the first-shell water molecules correctly. Note that the smaller Co−H distance is reflected in the second peak of the FT of $\chi(k)k^2$ signal in Figure 5, which is only a shoulder for CPMD data, whereas it is well-defined in the experimental one.

4.2. Second Hydration Shell. To understand the second hydration shell structure, a minimum box of 64 water molecules seems to be necessary in CPMD simulations. This means that a bigger computational effort is needed to obtain an accurate description of the second hydration shell. In fact, a unimodal distribution is observed for the CPMD-64 simulation, which is at variance with the CPMD-32 simulation. On the other hand, classical simulations provide the same value of second shell coordination number independently of the box used, probably because a larger temporal sampling supplies the lack of convergence that is due to the small number of molecules.

It is worth noting that experimental data on the second hydration shell are difficult to obtain at the same level of accuracy as the first hydration shell. Experimental data available in the literature are very widespread (the number of water molecules is in the range of 5.7−14.8 and the Co−O distance is in the range of 4.20−4.28 Å) and probably are strongly dependent on the experimental conditions,[1,76−79] where different complexes are present and the metal ion also is bound to non-solvent ligands (such as, i.e., Cl⁻ or acetate). The results of our CPMD simulations, which indicate 12.5 water molecules (on average) in the second coordination shell, are well within the experimental boundaries and provide a reasonable value for extreme dilute solutions. Note also that the second peak in the Co−O $g(r)$ distribution is very broad, providing a location with a large indeterminacy, but still in the correct region (i.e., in the region proposed from both experimental[1] and other theoretical studies[13,50]). Thus, a more-detailed analysis of the second hydration shell, coupling simulations with other experimental techniques as proposed in the following, seems necessary.

5. Conclusions

In the present work, we have investigated the hydration structure of Co²⁺ by means of Car−Parrinello molecular dynamics (CPMD) simulations and extended X-ray absorption fine structure (EXAFS) data analysis, based on the multiple-scattering theory. A detailed comparison between simulations and experiments was made and structural parameters on the first
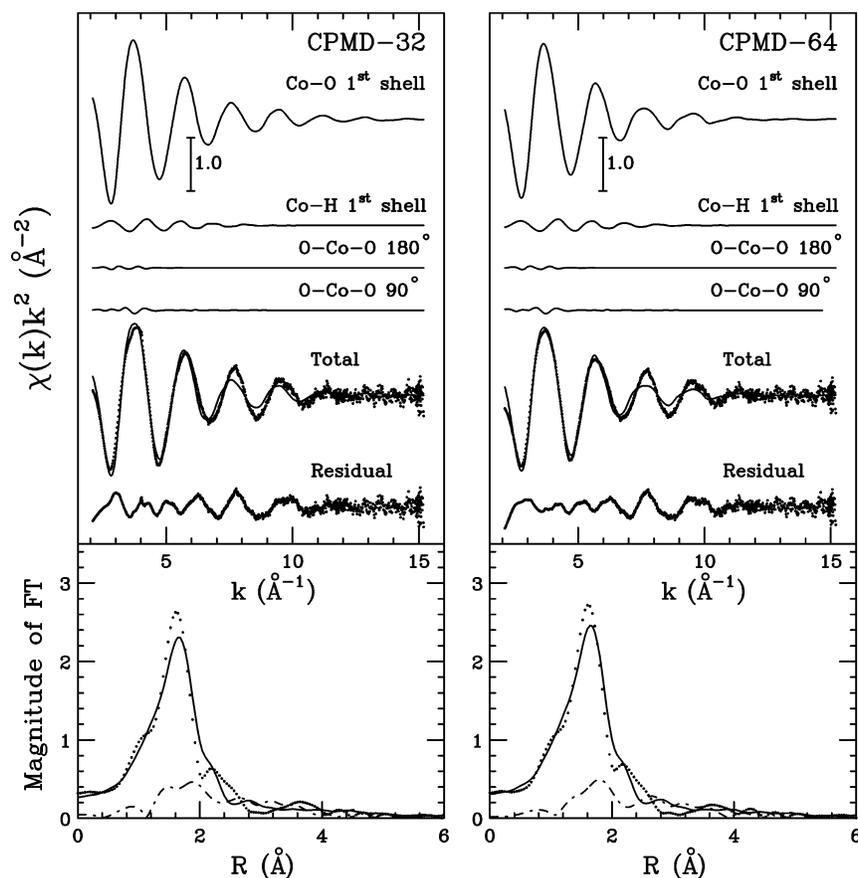
Figure 5. Upper panels: EXAFS signal calculated from CPMD-32 (left side) and CPMD-64 (right side) simulations (solid lines) and obtained from experiments (dotted lines). The residual signals (dashed−dotted lines) are also shown. Lower panels: the Fourier transforms of the calculated (solid lines), experimental (dotted lines), and residual (dashed−dotted lines) signals.

hydration shell were discussed in details, providing a good agreement between the two independent approaches. In particular here, for the first time, we have tested the reliability of DFT-based molecular dynamics (MD) in reproducing the experimental EXAFS signal and the corresponding first hydration shell properties. Results are encouraging. Furthermore, the second hydration shell structure was determined from simulations. Unfortunately, EXAFS cannot provide information on the second hydration shell. In this context, the analysis of the XANES region could overcome these limitations and provide information also on the second hydration shell,[15] as performed for Ni²⁺ using classical simulations.[80] Our work is moving in this direction, to couple XANES with Car−Parrinello simulations.

Finally, the Car−Parrinello setup developed here to describe Co²⁺ in aqueous solutions, together with previously reported results on cobalt−biomolecule interactions in the gas phase,[17] pave the way to study cobalt−biomolecular complexes in liquid water.

Appendix

EXAFS−CPMD Index of Agreement. The index of agreement between experimental ($\alpha_{exp}(E_i)$) and Car-Parrinello ($\alpha_{CPMD}(E_i)$) points is defined:

$$R_i = \sum_{i=1}^{N} \frac{[\alpha_{exp}(E_i) - \alpha_{CPMD}(E_i)]^2}{\sigma_i^2} \quad (3)$$

where N is the number of experimental points E_i and σ_i^2 is the variance associated with each experimental point $\alpha_{exp}(E_i)$. In most cases, σ_i^2 can be directly estimated from the experimental spectrum and a k^m weighting (with $m = 2, 3, ...$) results in a good approximation.[81]

Gamma Distribution Function. Peak shapes of calculated Co−O and Co−H radial distribution functions (RDFs) are modeled with gamma-like distribution curves with a mean distance R_m, a standard deviation σ, and asymmetry index β (the third cumulant divided by σ^3) $\beta = 2p^{-1/2}$ that can be gradually varied in a wide range. The general expression is

$$f(r) =$$
$$N_c \frac{p^{1/2}}{\sigma\Gamma(p)} \left[p + \left(\frac{r - R_m}{\sigma} \right) p^{1/2} \right]^{p-1} \exp\left[-p - \left(\frac{r - R_m}{\sigma} \right) p^{1/2} \right] \quad (4)$$

where $\Gamma(p)$ is the Euler's gamma function for the parameter p and N_c is the coordination number that provides the correct normalization.

Note that, as for the Gaussian distribution, the dumping of the $\chi(k)$ signal averaged over the gamma distribution can be

calculated exactly:[6]

$$\chi(k) = \mathrm{Im}\left\{A_0\, e^{i\psi_0}\left[1 + i\frac{A_1}{A_0}\frac{\psi_1\sigma^2}{(1 - i\psi_1\sigma p^{-1/2})}\right]\left[\frac{\exp(i\psi_1\sigma p^{1/2})}{(1 - i\psi_1\sigma p^{-1/2})^p}\right]\right\} \tag{5}$$

where $A_0 = A(k,R_\mathrm{m})$, $\psi_0 = \psi(k,R_\mathrm{m})$, $A_1 = \partial A(k,r)/\partial r|_{r=R_\mathrm{m}}$, and $\psi_1 = \partial\psi(k,r)/\partial r|_{r=R_\mathrm{m}}$, and Im indicates the imaginary part.

References and Notes

(1) Ohtaki, H.; Radnai, T. *Chem. Rev.* **1993**, *93,* 1157.

(2) Marcus, Y. *Chem. Rev.* **1988**, *88,* 1475.

(3) Johansson, G. *Adv. Inorg. Chem.* **1992**, *187,* 151.

(4) Hofer, T. S.; Tran, H. T.; Schwenk, C. F.; Rode, B. M. *J. Comput. Chem.* **2003**, *25,* 211.

(5) Rotzinger, F. P. *Chem. Rev.* **2005**, *105,* 2003.

(6) D'Angelo, P.; Di Nola, A.; Filipponi, A.; Pavel, N. V.; Roccatano, D. *J. Chem. Phys.* **1994**, *100,* 985.

(7) Roccatano, D.; Berendsen, H. J. C.; D'Angelo, P. *J. Chem. Phys.* **1998**, *108,* 9487.

(8) Dubois, V.; Archirel, P.; Boutin, A. *J. Phys. Chem. B* **2001**, *105,* 9363.

(9) Yagüe, J. I.; Mohammed, A. M.; Loeffler, H. H.; Rode, B. M. *J. Phys. Chem. A* **2001**, *105,* 7646.

(10) Rey, R.; Hynes, J. T. *J. Phys. Chem.* **1996**, *100,* 5611.

(11) Ferlat, G.; San Miguel, A.; Jal, J. F.; Soetsen, J. C.; Bopp, P. A.; Daniel, I.; Guillot, S.; Hazemann, J. L.; Argoud, R. *Phys. Rev. B* **2001**, *63,* 134202.

(12) Spangberg, D.; Rey, R.; Hynes, J. T.; Hermansson, K. *J. Phys. Chem. B* **2003**, *107,* 4470.

(13) Chillemi, G.; D'Angelo, P.; Pavel, N. V.; Sanna, N.; Barone, V. *J. Am. Chem. Soc.* **2002**, *124,* 1968.

(14) Chillemi, G.; Barone, V.; D'Angelo, P.; Mancini, G.; Persson, I.; Sanna, N. *J. Phys. Chem. B* **2005**, *109,* 9186.

(15) D'Angelo, P.; Roscioni, O. M.; Chillemi, G.; Della Longa, S.; M. Benfatto, M. *J. Am. Chem. Soc.* **2006**, *128,* 1853.

(16) Frank, I.; Parrinello, M.; Klamt, A. *J. Phys. Chem. A* **1998**, *102,* 3614.

(17) Spezia, R.; Tournois, G.; Tortajada, J.; Cartailler, T.; Gaigeot, M.-P. *Phys. Chem. Chem. Phys.* **2006**, *8,* 2040.

(18) Marinica, D. C.; Gregoire, G.; Desfrancois, C.; Schermann, J. P.; Borgis, D.; Gaigeot, M.-P. *J. Phys. Chem. A* **2006**, *110,* 8802.

(19) Sprik, M.; Hutter, J.; Parrinello, M. *J. Chem. Phys.* **1996**, *105,* 1142.

(20) Silvestrelli, P. L.; Parrinello, M. *J. Chem. Phys.* **1999**, *111,* 3572.

(21) Handgraaf, J. W.; Meijer, E. J.; Gaigeot, M.-P. *J. Chem. Phys.* **2004**, *121,* 10111.

(22) Rosso, L.; Tuckerman, M. E. *Solid State Ionics* **2003**, *161,* 219.

(23) Meregalli, V.; Parrinello, M. *Solid State Commun.* **2001**, *117,* 441.

(24) Lyubartsev, A. P.; Laasonen, K.; Laaksonen, A. *J. Chem. Phys.* **2001**, *114,* 3120.

(25) Marx, D.; Sprik, M.; Parrinello, M. *Chem. Phys. Lett.* **1997**, *273,* 360.

(26) Ramaniah, L.; Bernasconi, M.; Parrinello, M. *J. Chem. Phys.* **1998**, *109,* 6839.

(27) Vuilleumier, R.; Sprik, M. *J. Chem. Phys.* **2001**, *115,* 3454.

(28) White, J. A.; Schwegler, E.; Galli, G.; Gygi, F. *J. Chem. Phys.* **2000**, *113,* 4668.

(29) Lightstone, F. C.; Schwegler, E.; Hood, R. Q.; Gygi, F.; Galli, G. *Chem. Phys. Lett.* **2001**, *343,* 549.

(30) Lubin, M. I.; Bylaska, E. J.; Weare, J. H. *Chem. Phys. Lett.* **2000**, *322,* 447.

(31) Ramaniah, L.; Bernasconi, M.; Parrinello, M. *J. Chem. Phys.* **1999**, *111,* 1587.

(32) Bakó, I.; Hutter, J.; Pálinkás, G. *J. Chem. Phys.* **2002**, *117,* 9838.

(33) Ensing, B.; Baerends, E. J. *J. Phys. Chem. A* **2002**, *106,* 7902.

(34) Ensing, B.; Buda, F.; Blöch, P. E.; Baerends, E. J. *Phys. Chem. Chem. Phys.* **2002**, *4,* 3619.

(35) Pasquarello, A.; Petri, I.; Salomon, P. S.; Parisel, O.; Car, R.; Toth, E.; Powell, D. H.; Fischer, H. E.; Helm, L.; Merbach, A. *Science* **2001**, *291,* 856.

(36) Amira, S.; Spangberg, D.; Zelin, V.; Probst, M.; Hermansson, K. *J. Phys. Chem. B* **2005**, *109,* 14235.

(37) Yazyev, O. V.; Helm, L. *Theor. Chem. Acc.* **2006**, *115,* 190.

(38) Buhl, M.; Grigoleit, S.; Kabrede, H.; Mauschick, F. T. *Chem. Eur. J.* **2006**, *12,* 477−488.

(39) Raugei, S.; Klein, M. L. *J. Chem. Phys.* **2002**, *116,* 196.

(40) Spezia, R.; Nicolas, C.; Boutin, A.; Vuilleumier, R. *Phys. Rev. Lett.* **2003**, *91,* 208304.

(41) Ferlat, G.; Soetens, J.; San Miguel, A.; Bopp, P. A. *J. Phys.: Condens. Matter* **2005**, *17,* S145.

(42) Filipponi, A.; D'Angelo, P.; Pavel, N. V.; Di Cicco, A. *Chem. Phys. Lett.* **1994**, *225,* 150.

(43) D'Angelo, P.; Pavel, N. V. *J. Chem. Phys.* **1999**, *111,* 5107.

(44) Campbell, L.; Rehr, J. J.; Schenter, G. K.; McCarthy, M. I.; Dixon, D. *J. Synchrotron. Rad.* **1999**, *6,* 310.

(45) Benfatto, M.; Natoli, C. R.; Bianconi, A.; García, J.; Marcelli, A.; Fanfoni, M.; Davoli, I. *Phys. Rev. B* **1986**, *34,* 5774.

(46) D'Angelo, P.; Barone, V.; Chillemi, G.; Sanna, N.; Meyer-Klaucke, W.; Pavel, N. V. *J. Am. Chem. Soc.* **2002**, *124,* 1958.

(47) D'Angelo, P.; Chillemi, G.; Barone, V.; Mancini, G.; Sanna, N.; Persson, I. *J. Phys. Chem. B* **2005**, *109,* 9178.

(48) Ferlat, G.; San Miguel, A.; Xu, H.; Aouizerat, A.; Blase, X.; Zuniga, J.; Munoz-Sanjosé, V. *Phys. Rev. B* **2004**, *69,* 155202.

(49) Spezia, R.; Tournois, G.; Cartailler, T.; Tortajada, J.; Jeanvoine, Y. *J. Phys. Chem. A* **2006**, *110,* 9727.

(50) Armunanto, R.; Schwenk, C. F.; Bambang Satiaji, A. H.; Rode, B. M. *Chem. Phys. Lett.* **2003**, *295,* 63.

(51) Car, R.; Parrinello, M. *Phys. Rev. Lett.* **1985**, *55,* 2471.

(52) Marx, D.; Hutter, J. Ab Initio Molecular Dynamics: Theory and Implementation. In *Modern Methods and Algorithms of Quantum Chemistry*; Vol. 1; Grotendorst, J. Ed.; NIC Series; John von Meumann Institute for Computing: Jülich, Germany: 2000.

(53) Becke, A. D. *Phys. Rev. A* **1988**, *38,* 3098.

(54) Lee, C.; Yang, W.; Parr, R. G. *Phys. Rev. B* **1988**, *37,* 785.

(55) Cotton, F. A.; Wilkinson, G. *Advanced Inorganic Chemistry*; Wiley: New York, 1980.

(56) Trouillier, N.; Martins, J. L. *Phys. Rev. B* **1991**, *43,* 1993.

(57) Rovira, C.; Kunc, K.; Hutter, J.; Parrinello, M. *Inorg. Chem.* **2001**, *40,* 11.

(58) Kleinman, L.; Bylander, D. M. *Phys. Rev. Lett.* **1982**, *48,* 1425.

(59) Louie, S. G.; Froyen, S.; Cohen, M. L. *Phys. Rev. B* **1982**, *26,* 1738.

(60) Hutter, J.; Alavi, A.; Deutsch, T.; Bernasconi, M.; Goedecker, S.; Marx, D.; Tuckerman, M.; Parrinello, M. CPMD version 3.7.2; IBM Research Division, IBM Corp and Max Planck Institüt−Stuttgart.

(61) Grossman, J. C.; Schwegler, E.; Draeger, E. W.; Gygi, F.; Galli, G. *J. Chem. Phys.* **2004**, *120,* 300.

(62) Allen, M. P.; Tildesley, D. J. *Computer Simulation of Liquids*; Oxford Science Publications: Oxford, U.K., 1989.

(63) Souaille, M.; Borgis, D.; Gaigeot, M.-P. *MDVRY*; Molecular Dynamics Program Developed at the University of Evry: 2006.

(64) Berendsen, H. J. C.; Grigera, J. R.; Straatsma, T. P. *J. Phys. Chem.* **1987**, *91,* 6269.

(65) Cossi, M.; Rega, N.; Scalmani, G.; Barone, V. *J. Comput. Chem.* **2003**, *24,* 669.

(66) Hermes, C.; Gilberg, E.; Koch, M. H. *Nucl. Instrum. Methods Phys. Res.* **1984**, *222,* 207.

(67) Pettifer, R.; Hermes, C. *J. Phys. Colloq.* **1986**, *C8,* 127.

(68) Pettifer, R. F.; Hermes, C. *J. Appl. Crystallogr.* **1985**, *18,* 404.

(69) Filipponi, A.; Di Cicco, A.; Natoli, C. R. *Phys. Rev. B* **1995**, *52,* 15122.

(70) Hedin, L.; Lundqvist, B. I. *J. Phys. C* **1971**, *4,* 2064.

(71) Krause, M. O.; Oliver, J. H. *J. Phys. Chem. Ref. Data* **1979**, *8,* 329.

(72) Miheliuc, A.; Gomilusek, J. P.; Kodre, A.; Arucon, I. *HASYLAB Annual Report* **2000**, 209.

(73) Sham, T. K. *Acc. Chem. Res.* **1986**, *19,* 99.

(74) Miyanaga, T.; Sakane, H.; Watanabe, I. *Bull. Chem. Soc. Jpn.* **1995**, *68,* 819.

(75) Laage, D.; Hynes, J. T. *Science* **2006**, *311,* 832.

(76) Musinu, A.; Peschina, G.; Piccaluga, G.; Magini, M. *J. Chem. Phys.* **1984**, *80,* 2772.

(77) Magini, M. *J. Chem. Phys.* **1981**, *74,* 2523.

(78) Corrias, A.; Musinu, A.; Pinna, G. *Chem. Phys. Lett.* **1985**, *120,* 295.

(79) Caminiti, R.; Cucca, P.; Monduzzi, M.; Saba, G.; Crisponi, G. *J. Chem. Phys.* **1984**, *81,* 543.

(80) Roscioni, O. M.; D'Angelo, P.; Chillemi, G.; Della Longa, S.; Benfatto, M. *J. Synchrotron Rad.* **2005**, *12,* 75.

(81) Filipponi, A.; Di Cicco, A. *Phys. Rev. B* **1995**, *52,* 15135.